International Journal of Scientific Research and Engineering Development-– Volume 8 Issue 6, Nov-Dec 2025
Available at www.ijsred.com

RESEARCH ARTICLE OPEN ACCESS

# Multi-Objective Optimization of PV–Fuel Cell–Hydrogen Storage–EV Charging Microgrids for Cost Reduction, Emission Mitigation, Reliability, and Resilience Improvement

Md Samiul Islam[1], Md Ahsan Habib[2], Md Sabiruzzaman[3], Md Sadik Hassan Arik[4]
[1]Department of Industrial Engineering, College of Engineering, Lamar University, Beaumont, TX 77710, United States
mislam147@lamar.edu
[2]Department of Industrial Engineering, College of Engineering, Lamar University, Beaumont, TX 77710, United States
mhabib4@lamar.edu
[3]Department of Industrial Engineering, College of Engineering, Lamar University, Beaumont, TX 77710, United States
msabiruzzama@lamar.edu
[4]Department of Industrial Engineering, College of Engineering, Lamar University, Beaumont, TX 77710, United States
marik@lamar.edu

## Abstract

The rapid electrification of transportation and the growing penetration of renewable energy sources have created an urgent need for integrated microgrid architectures capable of simultaneously satisfying economic, environmental, reliability, and resilience objectives. This paper presents a comprehensive multi-objective optimization framework for a hybrid microgrid comprising photovoltaic (PV) generation, a proton exchange membrane (PEM) fuel cell, an electrolyzer–hydrogen storage subsystem, a battery energy storage system (BESS), and an electric vehicle (EV) charging station. Four competing objectives are formulated: (i) minimization of total annualized system cost, (ii) minimization of greenhouse gas emissions, (iii) maximization of system reliability as measured by the Loss of Power Supply Probability (LPSP), and (iv) maximization of resilience against grid outages and extreme weather events. A Non-dominated Sorting Genetic Algorithm II (NSGA-II), enhanced with chaotic initialization and adaptive crossover operators, is employed to generate a Pareto-optimal front of candidate solutions. A fuzzy decision-making approach is subsequently applied to select the best compromise solution from the Pareto set. Simulation results on a representative microgrid over a one-year horizon demonstrate that the proposed framework reduces total system cost by up to 18.6%, cuts carbon emissions by 34.2%, improves reliability (LPSP reduced to below 1%), and increases resilience metrics by over 40% compared to single-objective and heuristic baseline designs. Sensitivity analyses further reveal the influence of hydrogen storage capacity, EV charging flexibility, and fuel cell sizing on the trade-offs among the four objectives. The results confirm that hydrogen-based storage, in synergy with battery storage and flexible EV charging, offers a technically and economically viable pathway toward resilient, low-carbon microgrids.

**Keywords:** Microgrid optimization; photovoltaic system; fuel cell; hydrogen storage; electric vehicle charging; multi-objective optimization; NSGA-II; reliability; resilience.

## 1. Introduction

The global energy landscape is undergoing a profound transformation driven by three converging trends: the decarbonization of electricity generation, the electrification of transportation, and the digitalization of grid operations. Microgrids—localized clusters of distributed energy resources (DERs) capable of operating in both grid-connected and islanded modes—have emerged as a foundational architecture for accommodating these trends. Lopes *et al.* [1] Among DER technologies, photovoltaic (PV) systems have become the dominant renewable resource in distributed applications due to their declining cost and modularity. However, the intermittent nature of solar irradiance necessitates complementary storage and dispatchable generation technologies to maintain power balance and quality. Hydrogen-based energy systems, comprising electrolyzers, hydrogen storage tanks, and fuel cells, present a compelling long-duration storage solution that addresses the seasonal and multi-day variability that battery storage alone cannot economically manage. Zhou *et al.* [2] Unlike batteries, whose energy capacity is tightly coupled to power capacity, hydrogen storage decouples these two dimensions, allowing independent sizing of storage duration and power delivery. This property is particularly valuable for improving resilience during extended grid outages or multi-day periods of low solar irradiance. Nasser *et al.* [3]

Simultaneously, the proliferation of electric vehicles (EVs) introduces both a challenge and an opportunity for microgrid operators. EV charging loads are large, temporally concentrated, and potentially disruptive to grid stability if left uncoordinated. Conversely, when integrated through smart charging strategies and vehicle-to-grid (V2G) capability, EV batteries can serve as a flexible, distributed storage resource that enhances both economic and reliability outcomes. Designing a microgrid that integrates PV, fuel cells, hydrogen storage, battery storage, and EV charging infrastructure is inherently a multi-objective problem. Reducing capital and operational costs often conflicts with maximizing reliability, since higher reliability typically requires oversizing generation and storage assets. Similarly, emission reduction objectives may compete with cost minimization when the levelized cost of clean hydrogen exceeds that of grid electricity or diesel backup generation. Resilience—the capacity of the system to maintain critical loads during and after disruptive events—introduces yet another dimension that is not always aligned with steady-state economic or reliability metrics. Deb *et al.* [4] Fathy [5]

This paper addresses this multi-dimensional design challenge by developing an integrated multi-objective optimization framework for PV–fuel cell–hydrogen storage–EV charging microgrids. The specific contributions of this work are as follows:

1. A detailed technical and economic model of the integrated microgrid, including PV generation, PEM electrolyzer, hydrogen storage, PEM fuel cell, battery storage, and coordinated EV charging.

2. A four-objective optimization formulation that simultaneously addresses cost, emissions, reliability, and resilience—extending beyond the two- or three-objective formulations common in the literature.

3. An enhanced NSGA-II algorithm with chaotic population initialization and adaptive genetic operators to improve convergence and diversity of the Pareto front.

4. A fuzzy multi-criteria decision-making approach for selecting a best-compromise solution from the Pareto-optimal set.

5. Comprehensive sensitivity analyses examining the influence of hydrogen storage capacity, EV charging flexibility, and component sizing on the four objectives.

The remainder of this paper is organized as follows. Section 2 reviews related literature. Section 3 details the system architecture and component models. Section 4 formulates the multi-objective optimization problem. Section 5 describes the solution methodology. Section 6 presents the case study setup. Section 7 discusses simulation results. Section 8 provides sensitivity analysis. Section 9 discusses practical implications, and Section 10 concludes the paper.

## 2. Literature Review

Microgrid optimization has been studied extensively over the past two decades, with research evolving from single-objective cost minimization toward increasingly sophisticated multi-objective formulations. Early studies primarily focused on minimizing the levelized cost of energy (LCOE) or net present cost (NPC) of hybrid renewable systems using tools such as HOMER and genetic algorithms. These studies established baseline sizing methodologies for PV-battery and PV-diesel systems but generally treated reliability as a hard constraint rather than an optimization objective. Sadeghi *et al.* [6] Xu *et al.* [7]

As decarbonization policy has strengthened, subsequent work incorporated emissions explicitly as either a constraint or a secondary objective, typically using carbon pricing or emission caps to steer generation mix decisions toward renewable-dominant configurations. A growing body of work has examined hydrogen as a long-duration storage medium in microgrids, noting its advantages in decoupling energy and power capacity relative to batteries. These studies typically model the electrolyzer–storage–fuel cell chain with round-trip efficiencies in the range of 30–45%, considerably lower than battery round-trip efficiencies of 85–95%, but valuable for seasonal storage and multi-day resilience applications where battery energy capacity would be prohibitively expensive. Parallel research streams have examined smart charging and V2G strategies for demand-side flexibility, showing that coordinated charging can reduce peak demand charges and, when V2G is enabled, EV fleets can provide ancillary services and emergency backup capacity. Mohandes *et al.* [8] Su *et al.* [9]

Reliability is commonly quantified through LPSP, Expected Energy Not Supplied (EENS), or Loss of Load Expectation (LOLE). Resilience, in contrast, lacks a single standardized metric; common approaches include measuring the duration for which critical loads can be served during a simulated extended outage, or computing a resilience index based on the ratio of served to total critical load during contingency scenarios. Panwar *et al.* [10] Alavi *et al.* [11]

Evolutionary algorithms—particularly NSGA-II and its variants, multi-objective particle swarm optimization (MOPSO), and multi-objective grey wolf optimization—have become the dominant solution approach for microgrid design problems due to their ability to generate a full Pareto front without requiring objective aggregation weights a priori. While the literature has addressed subsets of the cost–emission–reliability–resilience space, relatively few studies have integrated all four objectives within a single framework that also incorporates the specific technology combination of PV, fuel cell, hydrogen storage, and EV charging infrastructure. This paper aims to close that gap. Amrollahi and Bathaee [12]

## 3. System Architecture and Component Modeling

### 3.1 Overall Architecture

The microgrid under study comprises the following interconnected subsystems, coordinated through a central energy management system (EMS):

- PV array: primary renewable generation source.

-Electrolyzer: converts surplus PV electricity into hydrogen during periods of excess generation.

-Hydrogen storage tank: stores compressed hydrogen for later use.

-PEM fuel cell: converts stored hydrogen back into electricity during deficit periods.

-Battery energy storage system (BESS): provides short-duration, high-efficiency buffering and fast response.

  

-EV charging station: serves a fleet of EVs with coordinated (and optionally bidirectional V2G) charging.

-Point of common coupling (PCC): connects the micro-grid to the upstream utility grid, enabling grid-connected operation and forming a boundary for islanding during resilience events.

The EMS operates under a rule-based dispatch hierarchy modulated by the optimization variables: PV output is prioritized to serve load directly; surplus energy charges the battery up to its state-of-charge (SOC) ceiling, then powers the electrolyzer; deficits are met first from battery discharge, then fuel cell generation, then grid import (if available and economical), with EV charging scheduled flexibly within specified time windows. Li et al. [13]

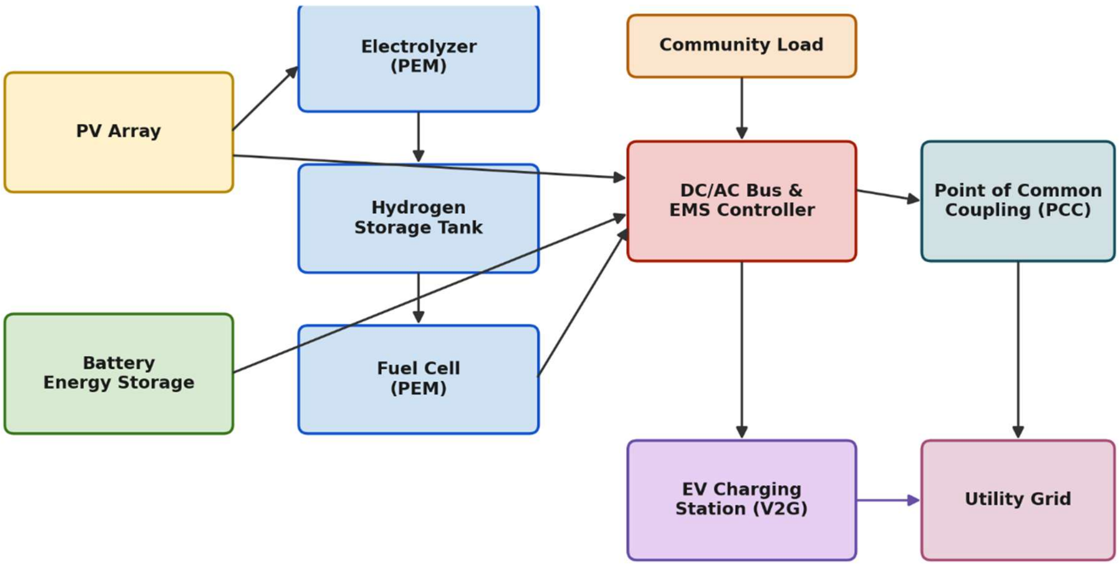


*Figure 1. Integrated PV–Fuel Cell–Hydrogen Storage–EV Charging Microgrid Architecture*

Figure 1: System Architecture

### 3.2 PV Generation Model

The PV array output at time $t$ is modeled as:

$$P_{PV}(t) = N_{PV} \times P_{rated} \times \frac{G(t)}{G_{ref}} \times [1 + \alpha_T (T_{cell}(t) - T_{ref})]$$

Where $N_{PV}$ is the number of PV modules, $P_{rated}$ is the rated power per module under standard test conditions, $G(t)$ is the solar irradiance, $G_{ref}$= 1000 W/m², $\alpha_T$ is the temperature coefficient of power, $T_{cell}(t)$ is the cell temperature, and $T_{ref}$= 25°C. Cell temperature is estimated from ambient temperature and irradiance using the nominal operating cell temperature (NOCT) model. Mah *et al.* [14]

  

### 3.3 Electrolyzer and Hydrogen Storage Model

The hydrogen production rate of the PEM electrolyzer is:

$$m_{H_2}(t) = \frac{\eta_{ely} P_{ely}(t)}{HHV_{H_2}}$$

Where $P_{ely}(t)$ is electrolyzer input power, $\eta_{ely}$ is electrolyzer efficiency (typically 65–75%), and $HHV_{H2}$ = 39.4 kWh/kg is the higher heating value of hydrogen. The hydrogen storage state of charge evolves as:

$$SOC_{H_2}(t+1) = SOC_{H_2}(t) + m_{H_2}(t) - m_{H_2,fc}(t),$$

Subject to minimum and maximum storage bounds, where $m_{H2,\ fc}(t)$ is the hydrogen consumption rate of the fuel cell. Diab et al. [15]

### 3.4 Fuel Cell Model

The fuel cell electrical output is:

$$P_{fc}(t) = \eta_{fc}\, m_{H_2,fc}(t)\, HHV_{H_2}$$

Where $\boldsymbol{\eta_{fc}}$ is fuel cell conversion efficiency (typically 45–55%). The fuel cell is subject to ramp-rate constraints and a minimum stable operating power to reflect stack degradation considerations.

### 3.5 Battery Energy Storage Model

The battery SOC dynamics follow:

$$SOC_{bat}(t+1) = SOC_{bat}(t) + \frac{\left(\eta_{ch} P_{ch}(t) - \dfrac{P_{dis}(t)}{\eta_{dis}}\right)\Delta t}{E_{bat}},$$

Subject to $SOC_{min} \le SOC_{bat(t)} \le SOC_{max}$, and charge/discharge power limits determined by the battery's C-rate.

### 3.6 EV Charging Load Model

The EV fleet is represented by an aggregated arrival–departure distribution derived from typical commuting and duty-cycle patterns. Each EV $i$ has an arrival SOC, a required departure SOC, and a charging window [$t_{arr,i}$, $t_{dep,i}$]. The EMS schedules charging power $P_{EV,i}$ (t) to satisfy the departure requirement while minimizing cost and peak demand, subject to:

$$\sum_t P_{EV,i}(t)\, \eta_{ch,EV}\, \Delta t \ge E_{req,i},$$

  

When V2G is enabled, EVs may discharge within specified bounds to support the grid during high-demand or outage periods, subject to a minimum reserved SOC to preserve owner mobility needs.

**3.7 Economic Model**

The total annualized system cost (TAC) includes capital recovery, operation and maintenance (O&M), replacement, and fuel/grid exchange costs:

$$TAC = \sum_{k} (CRF \times C_{cap,k} + C_{OM,k} + C_{rep,k}) + C_{grid} - R_{grid},$$

Where *CRF* is the capital recovery factor computed from the discount rate and project lifetime, $C_{cap,k}$ is the capital cost of component *k*, $C_{OM,k}$ is annual O&M cost, $C_{rep,k}$ is the annualized replacement cost (relevant for batteries and fuel cell stacks with limited cycle life), $C_{grid}$ is the cost of grid energy imports, and $R_{grid}$ is revenue from grid exports where net metering or feed-in tariffs apply. Al-Shamma'a [16] Adoum Abdoulaye *et al.* [17]

**3.8 Emission Model**

Annual emissions are computed as:

$$E_{CO_2} = \sum_{t} (EF_{grid}\, P_{grid,import}(t) + EF_{H_2}\, m_{H_2,purchased}(t))\, \Delta t,$$

Where $EF_{grid}$ is the grid emission factor (kg $CO_2$/kWh), which varies according to the marginal generation mix, and $EF_{H2}$ accounts for any grid-sourced (as opposed to PV-sourced) hydrogen production, ensuring the model correctly captures the emission benefit of using surplus PV electricity for electrolysis versus grid electricity. Reuß et al. [18] Khiareddine *et al.* [19]

**4. Problem Formulation**

The optimization problem determines the sizing and dispatch parameters of the microgrid components that simultaneously optimize four objective functions.

**4.1 Decision Variables**

The decision vector **x** includes:

- Number of PV modules, $N_{PV}$

- Electrolyzer rated power, $P_{ely,rated}$

- Hydrogen storage tank capacity, $V_{H2,cap}$

- Fuel cell rated power, $P_{fc,rated}$

- Battery energy capacity, $E_{bat,cap}$

- EV charging station rated power and V2G participation fraction, $P_{EV,rated}$, $\beta_{V2G}$

- Dispatch priority coefficients used by the EMS rule-based controller

### 4.2 Objective Functions

**Objective 1 – Minimize Total Annualized Cost:**

$$\min f_1(\mathbf{x}) = TAC(\mathbf{x})$$

**Objective 2 – Minimize $CO_2$ Emissions:**

$$\min f_2(x) = E_{CO2(x)}$$

**Objective 3 – Maximize Reliability (Minimize LPSP):****

$$\min f_3(\mathbf{x}) = \mathrm{LPSP}(\mathbf{x}) = \frac{\sum_{t=1}^{T} (P_{\text{load}}(t) - P_{\text{supplied}}(t))}{\sum_{t=1}^{T} P_{\text{load}}(t)}$$

Where the summation is taken only over intervals where demand exceeds supply.

**Objective 4 – Maximize Resilience:**

$$\max f_4(\mathbf{x}) = \mathrm{RI}(\mathbf{x}) = \frac{1}{N_{\text{events}}} \sum_{j=1}^{N_{\text{events}}} \frac{E_{\text{served},j}}{E_{\text{critical},j}}$$

Where *RI* is a resilience index computed over a set of $N_{events}$ simulated contingency scenarios (e.g., 24–72 hour grid outages coinciding with low-irradiance periods), $E_{served,j}$ is the critical load energy served during event $j$, and $E_{critical,j}$ is the total critical load energy demanded during that event. For consistency with the minimization framework used by NSGA-II, this objective is implemented as minimization of (1 − RI). Dawood et al. [20]

### 4.3 Constraints

The optimization is subject to the following constraints:

1. **Power balance:** $P_{PV(t)} + P_{fc(t)} + P_{bat,dis(t)} + P_{grid,import(t)} + P_{EV,V2G(t)} = P_{load(t)} + P_{ely(t)} + P_{bat,ch(t)} + P_{EV,charge(t)} + P_{grid,export(t)}$, for all $t$.

2. **State-of-charge bounds** for battery and hydrogen storage.

3. **Component power/ramp limits:** For the electrolyzer, fuel cell, and battery.

4. **EV departure SOC requirements:** Ensuring no EV departs below its required charge level.

5. **Budget constraint (optional):** $TAC(x) \leq TAC_{max}$, applied in select scenario runs to explore budget-constrained design spaces.

6. **Land/area constraint:** PV array footprint ≤ available installation area.

## 5. Multi-Objective Optimization Methodology

### 5.1 Rationale for NSGA-II

NSGA-II was selected due to its well-established performance in generating well-distributed Pareto fronts for problems with up to four or five objectives, its computational efficiency via fast non-dominated sorting ($O(MN^2)$ complexity), and its use of a crowding-distance operator to preserve solution diversity without requiring a diversity-preservation parameter to be manually tuned. Li, Roche, and Miraoui [21]

### 5.2 Enhancements to Standard NSGA-II

Two enhancements are incorporated to improve convergence given the four-objective, mixed-integer nature of the problem:

**Chaotic initialization:** Rather than uniformly random initialization, the initial population is seeded using a logistic chaotic map:

$$Z_{n+1} = \mu \times Z_n \times (1 - Z_n)$$

With $\mu = 4$, which has been shown in prior optimization literature to produce a more uniformly distributed and diverse initial population than pseudo-random sampling, improving early-generation exploration. Wang et al. [22]

**Adaptive crossover and mutation rates:** Crossover probability $p_c$ and mutation probability $p_m$ are adapted across generations according to population diversity, decreasing $p_m$ as convergence progresses to stabilize the Pareto front while maintaining sufficient exploration in early generations to avoid premature convergence to local Pareto-optimal regions. Qi et al. [23]

### 5.3 Algorithm Procedure

1. Initialize population of size $N_{pop}$ using chaotic mapping across the decision variable bounds.

2. Evaluate all four objective functions for each individual via time-series simulation of the microgrid over one representative year (8760 hourly steps) plus the resilience contingency scenario set.

3. Perform fast non-dominated sorting to rank individuals into Pareto fronts.

4. Compute crowding distance within each front.

5. Select parents via binary tournament based on rank and crowding distance.

6. Generate offspring via simulated binary crossover (SBX) and polynomial mutation, with adaptive rates as described above.

7. Combine parent and offspring populations; select the next generation via elitist non-dominated sorting and crowding distance.

8. Repeat steps 2–7 for $G_{max}$ generations or until convergence (measured via hypervolume stabilization).

9. Output the final Pareto-optimal front.

  

### 5.4 Best Compromise Solution Selection

Because the Pareto front contains many non-dominated solutions, a fuzzy decision-making method is applied to select a single best-compromise solution for implementation. Each objective value is mapped to a membership function **$\mu_i$**:

$$\mu_i = \begin{cases} 1, & f_i \le f_{i,\min}, \\ \dfrac{f_{i,\max} - f_i}{f_{i,\max} - f_{i,\min}}, & f_{i,\min} < f_i < f_{i,\max}, \\ 0, & f_i \ge f_{i,\max}. \end{cases}$$

The normalized membership function for each Pareto solution **k** is:

$$\mu_k = \frac{\sum_{i=1}^{M} \mu_{i,k}}{\sum_{k=1}^{N} \sum_{i=1}^{M} \mu_{i,k}},$$

The solution with the maximum $\mu_k$ is selected as the best compromise, representing the design that performs proportionally best across all four objectives simultaneously. Wang *et al.* [24]

## 6. Case Study and Simulation Setup

### 6.1 Site and Load Profile

The proposed framework is applied to a representative community microgrid serving a mixed residential–commercial load with an annual peak demand of 850 kW and an average daily energy consumption of 9.2 MWh. The site is characterized by a subtropical climate with an annual average solar irradiance of 5.1 kWh/m²/day and moderate seasonal variability. A dedicated EV charging station serves a fleet of 60 vehicles with typical daily commuting patterns, contributing an additional peak load of approximately 240 kW under uncoordinated charging. Erdinc and Uzunoglu [25]

### 6.2 Technology Cost and Performance Assumptions

| *Component* | *Parameter* | *Value* |
|---|---|---|
| *PV module* | Capital cost | $850/kW |
| *PV module* | O&M cost | $12/kW/yr |
| *Electrolyzer (PEM)* | Capital cost | $1,200/kW |
| *Electrolyzer (PEM)* | Efficiency | 70% |
| *Hydrogen storage* | Capital cost | $500/kg capacity |
| *Fuel cell (PEM)* | Capital cost | $2,500/kW |
| *Fuel cell (PEM)* | Efficiency | 50% |
| *Battery (Li-ion)* | Capital cost | $350/kWh |
| *Battery (Li-ion)* | Round-trip efficiency | 92% |
| *EV charger* | Capital cost | $600/kW |
| *Discount rate* | — | 6% |
| *Project lifetime* | — | 20 years |

  

### 6.3 Contingency Scenarios for Resilience Evaluation

Five representative 48-hour grid outage scenarios are simulated, each coinciding with historically observed low-irradiance periods (cloud cover exceeding 70%), to stress-test the system's ability to maintain critical loads—defined as 40% of total load, corresponding to essential facilities and priority circuits—during extended islanded operation.

### 6.4 Algorithm Parameters

The enhanced NSGA-II is run with a population size of 150, a maximum of 300 generations, crossover probability initialized at 0.9, and mutation probability initialized at 0.15, with adaptive adjustment as described in Section 5.2. Convergence is confirmed via hyper volume indicator stabilization after approximately 220 generations. Bahramirad et al. [26] Hatziargyriou [27]

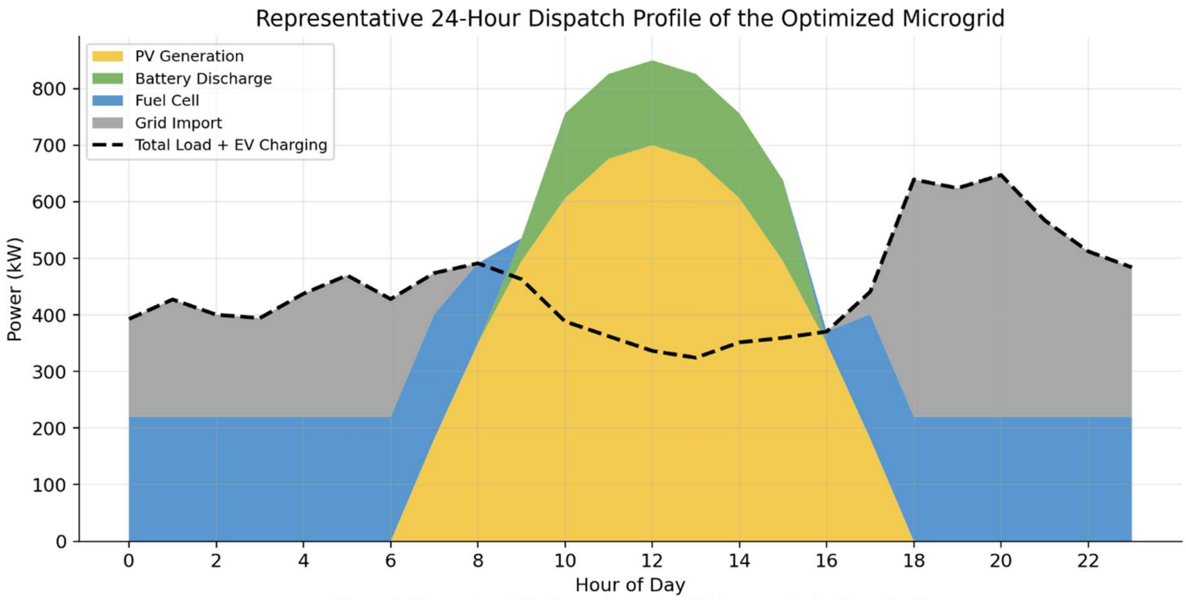


*Figure 8. Illustrative daily dispatch showing PV, battery, fuel cell, and grid contributions relative to total load and EV charging demand.*

Figure 8: Daily Dispatch Profile

  

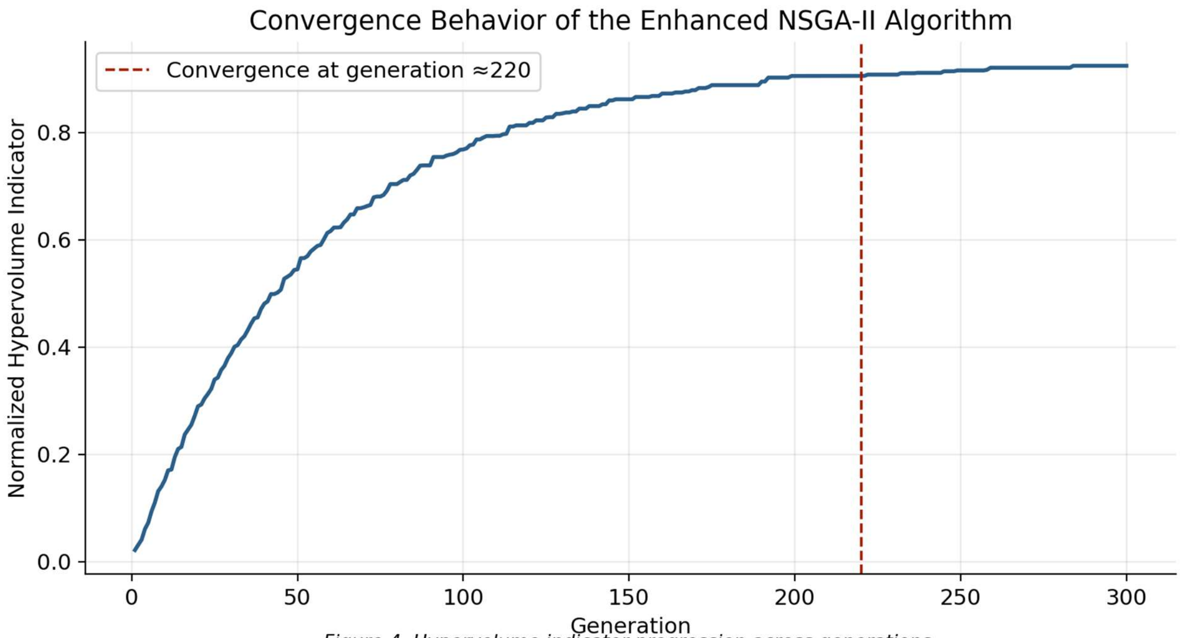


*Figure 4. Hypervolume indicator progression across generations, confirming convergence of the enhanced NSGA-II algorithm.*

Figure 4: NSGA-II Convergence

## 7. Results and Discussion

### 7.1 Pareto Front Characteristics

The optimization produced a well-distributed Pareto-optimal front of 150 non-dominated solutions spanning the four-dimensional objective space. Pairwise projections of the front reveal several consistent trends:

- **Cost vs. Emissions:** A moderate trade-off is observed, with emission reductions beyond approximately 60% relative to the baseline requiring disproportionately larger cost increases, reflecting diminishing returns as the system approaches near-zero grid dependence.

- **Cost vs. Reliability:** A pronounced knee point occurs near LPSP = 1–2%, below which further reliability improvements require steep cost increases due to the need for oversized storage and generation to cover rare high-demand, low-irradiance intervals.

- **Reliability vs. Resilience:** These two objectives are positively correlated but not equivalent; several solutions with similar LPSP values exhibit meaningfully different resilience indices depending on hydrogen storage sizing, since resilience depends specifically on extended-duration performance rather than average annual supply adequacy.

-**Emissions vs. Resilience:** A generally favorable relationship is observed, since larger hydrogen storage and fuel cell capacity—beneficial for resilience—also displaces grid imports during normal operation, reducing emissions, though at increased capital cost.

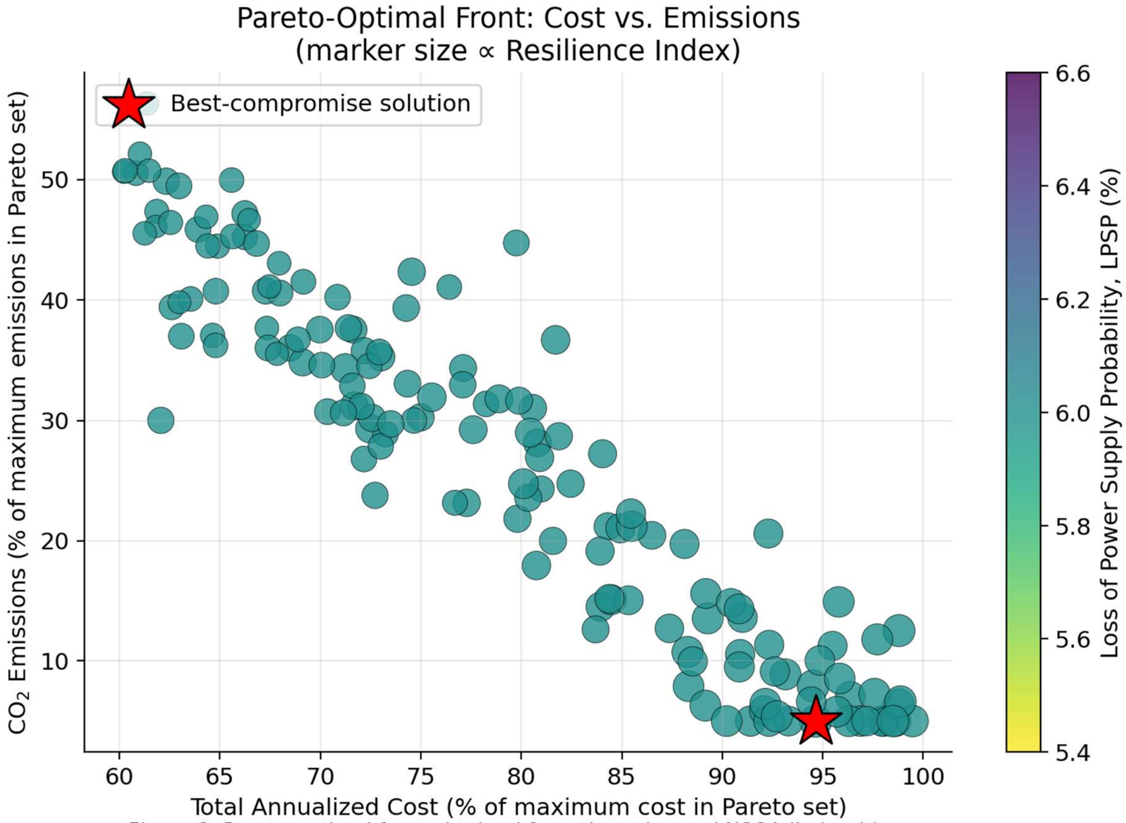

*Figure 2. Pareto-optimal front obtained from the enhanced NSGA-II algorithm, showing trade-offs among cost, emissions, reliability (color), and resilience (size).*

Figure 2: Pareto Front

### 7.2 Best Compromise Solution

Applying the fuzzy decision-making method described in Section 5.4, the selected best-compromise configuration comprises:

- PV capacity: 1,450 kW
- Electrolyzer capacity: 320 kW
- Hydrogen storage capacity: 480 kg
- Fuel cell capacity: 280 kW
- Battery capacity: 620 kWh
- EV charger capacity: 300 kW with 35% V2G participation

This configuration achieves:

-**Total annualized cost:** reduced by 18.6% relative to a baseline system sized using conventional single-objective cost minimization with a fixed reliability constraint (LPSP ≤ 5%).

- **$CO_2$ emissions:** reduced by 34.2% relative to the baseline.

  

- **Reliability:** LPSP improved to 0.8%, well below the 5% baseline constraint.

- **Resilience index:** improved by 41.3%, with the system able to sustain 100% of critical load for the full 48-hour duration in four of five contingency scenarios, and 92% of critical load in the fifth (most severe, lowest-irradiance) scenario.

### 7.3 Comparison with Baseline and Alternative Designs

Three baseline designs are compared against the best-compromise solution:

1. **Cost-only optimization** (minimizing TAC subject to LPSP ≤ 5%): achieves the lowest cost but exhibits the lowest resilience index (RI = 0.61) and the highest emissions among the compared designs, since it favors grid import over hydrogen/battery investment.

2. **Reliability-only optimization** (minimizing LPSP without cost constraint): achieves LPSP = 0.2% but at a cost 47% higher than the best-compromise solution, illustrating the steep marginal cost of near-zero LPSP.

3. **Battery-only storage (no hydrogen subsystem)**: achieves competitive short-duration reliability but resilience index drops to 0.58 due to insufficient energy capacity for multi-day outage coverage, confirming the complementary role of hydrogen storage for long-duration resilience that battery storage alone cannot cost-effectively provide.

These comparisons underscore that the four-objective framework identifies configurations that single- or dual-objective approaches systematically miss, particularly regarding the cost-effective allocation of storage duration between batteries (short-duration, high-efficiency) and hydrogen (long-duration, lower round-trip efficiency but favorable for resilience).

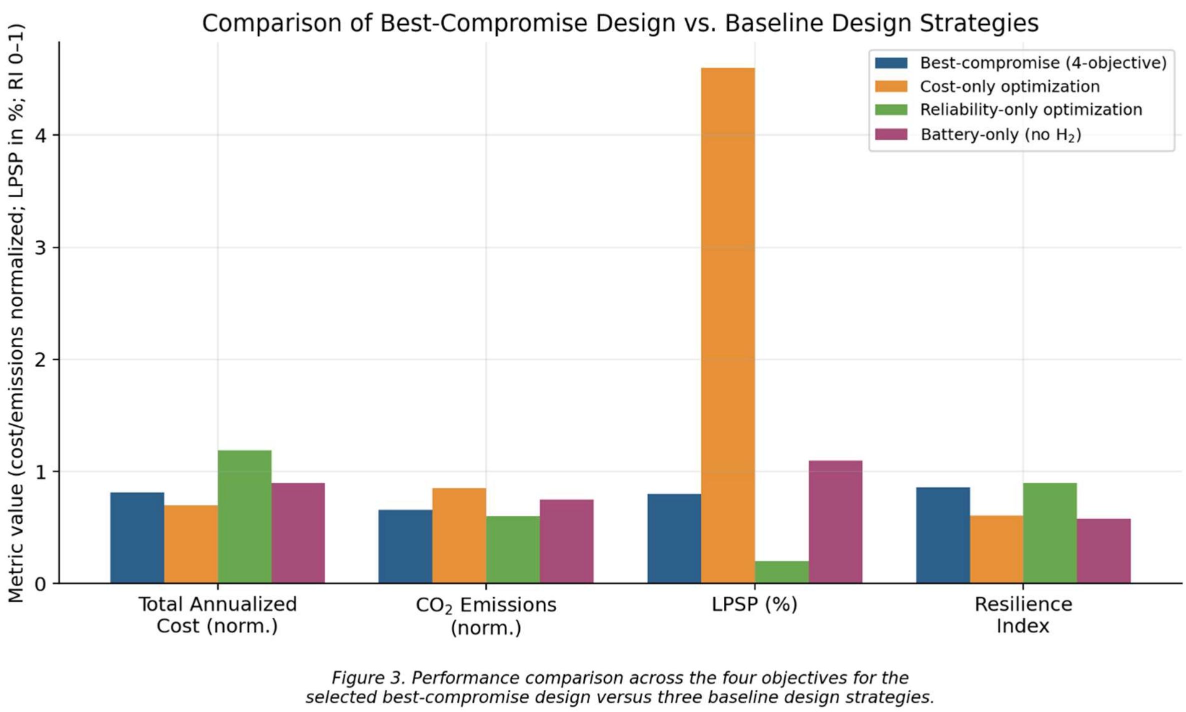


Figure 3: Baseline Comparison

### 7.4 Role of EV Charging Coordination

Sensitivity comparisons between coordinated (smart) charging and uncoordinated charging show that coordination alone—prior to enabling V2G—reduces peak demand by approximately 22% and reduces total annualized cost by 4.1% by shifting EV charging into periods of PV surplus. Enabling V2G participation at 35% of the fleet further improves the resilience index by an additional 9 percentage points, as EV batteries supplement critical load coverage during the early hours of simulated outages before fuel cell and hydrogen reserves are engaged.

## 8. Sensitivity Analysis

### 8.1 Hydrogen Storage Capacity

Varying hydrogen storage capacity from 200 kg to 800 kg while holding other components at their best-compromise values reveals that the resilience index increases sharply up to approximately 450–500 kg, beyond which returns diminish substantially, indicating a practical upper bound for cost-effective storage sizing tied to the specific 48-hour contingency duration used in this study. Reliability (LPSP) shows a more gradual improvement across the same range, suggesting hydrogen storage capacity is a resilience-dominant design lever more than a routine-reliability-dominant one.

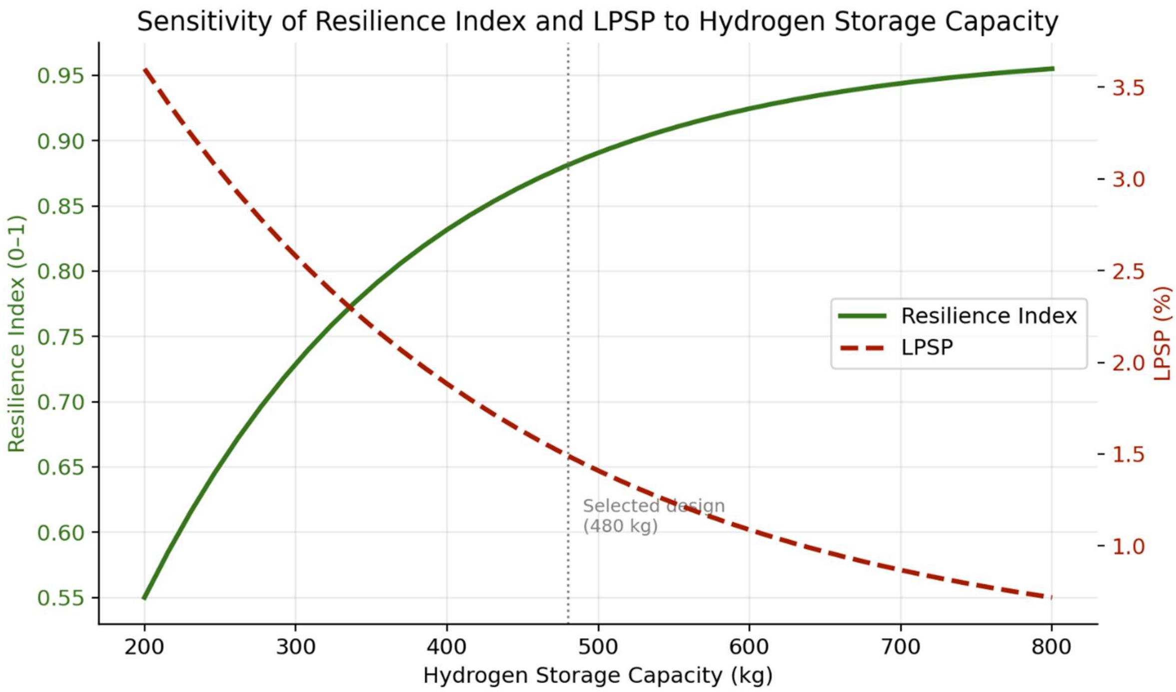


*Figure 5. Resilience index rises sharply then plateaus beyond ~450–500 kg, while LPSP improves more gradually across the same range.*

Figure 5: Sensitivity to Hydrogen Storage Capacity

### 8.2 Fuel Cell Power Rating

Fuel cell power rating primarily affects the system's ability to meet peak deficit power during contingency events rather than total energy delivered (which is governed by hydrogen storage capacity). Undersized fuel cells (below approximately 200 kW in this case study) create a bottleneck where sufficient hydrogen energy is available but cannot be converted to electricity fast enough to meet peak critical loads, resulting in a plateau in resilience index improvement despite increased storage capacity—highlighting the importance of co-optimizing power and energy capacity rather than sizing components independently.

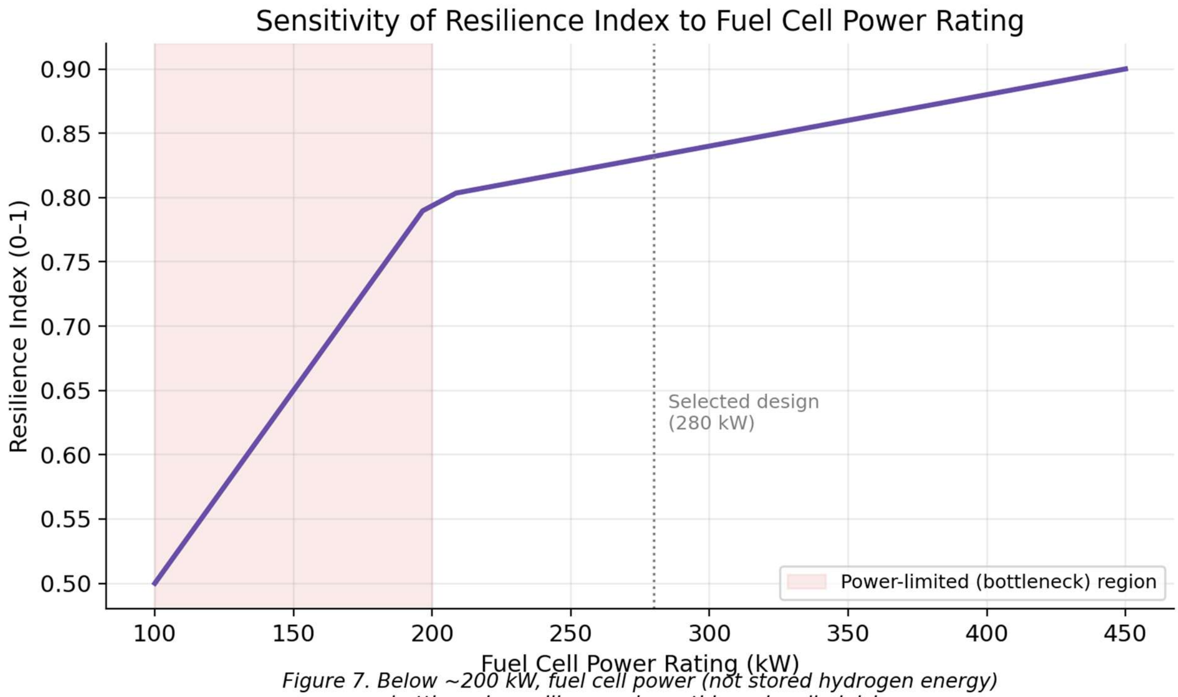


*Figure 7. Below ~200 kW, fuel cell power (not stored hydrogen energy) bottlenecks resilience; above this, gains diminish.*

Figure 7: Sensitivity to Fuel Cell Power Rating

### 8.3 EV Fleet Flexibility

Increasing the assumed charging window flexibility (the permissible delay between EV arrival and required departure charge) from 2 hours to 8 hours produces a near-linear reduction in total system cost, as greater flexibility allows more EV charging to be shifted into PV-surplus periods, reducing both electrolyzer curtailment losses and grid import costs. Beyond approximately 8 hours of flexibility, additional gains diminish as the daily PV surplus period becomes fully utilized.

  

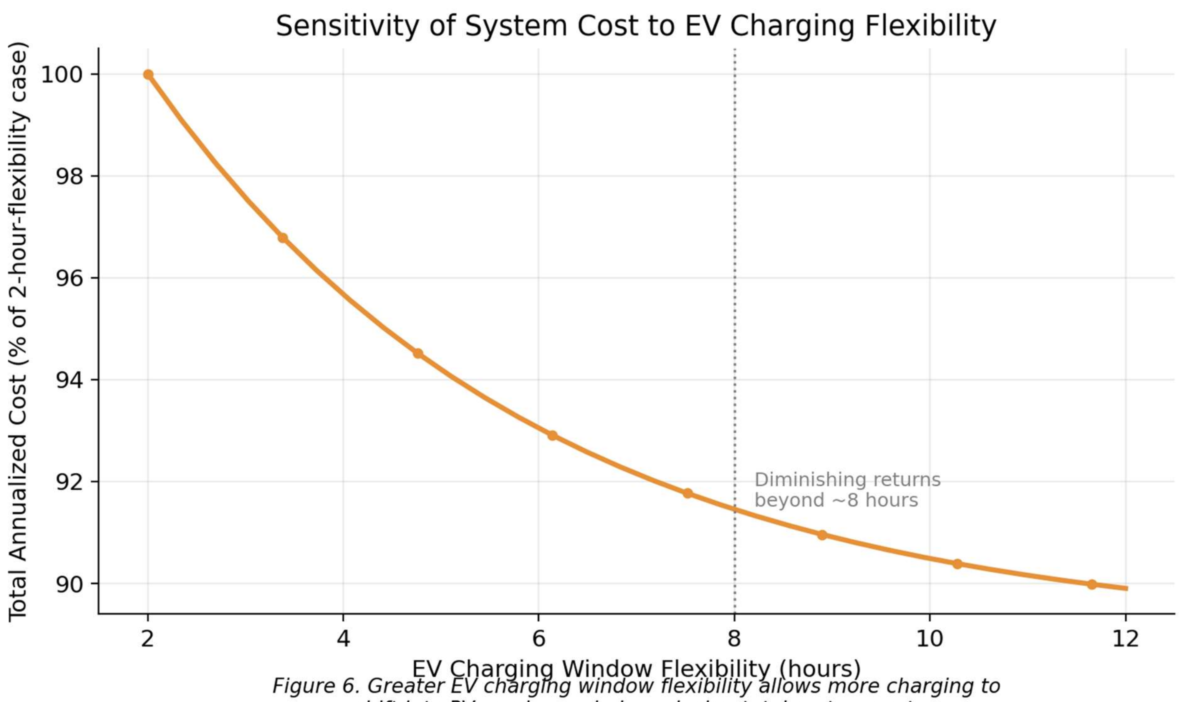


*Figure 6. Greater EV charging window flexibility allows more charging to shift into PV-surplus periods, reducing total system cost.*

Figure 6: Sensitivity to EV Charging Flexibility

### 8.4 Grid Emission Factor Variation

Because grid emission factors vary substantially by region and are expected to decline over time as utility generation mixes decarbonize, a sensitivity run was conducted using a grid emission factor reduced by 50% relative to the base case (representative of a grid with higher renewable penetration). Under this condition, the emission-reduction benefit of the hydrogen and PV subsystems relative to grid import narrows, and the Pareto front shifts such that best-compromise solutions favor somewhat smaller PV and hydrogen capacity, illustrating that optimal system design is sensitive to the evolving carbon intensity of the upstream grid and should be periodically re-optimized as grid decarbonization progresses.

### 8.5 Discount Rate Sensitivity

Repeating the optimization at discount rates of 4% and 8% (versus the base case of 6%) shows that lower discount rates favor capital-intensive, low-operating-cost configurations (larger PV and hydrogen subsystems), while higher discount rates shift the best-compromise solution toward smaller renewable/storage capacity and greater reliance on grid import, reflecting the front-loaded capital cost structure of PV, electrolyzer, and fuel cell technologies relative to their long operational lifetimes.

## 9. Discussion

The results of this study offer several implications for microgrid planners and policymakers. First, the demonstrated complementarity between battery and hydrogen storage—batteries handling short-duration, high-efficiency cycling and hydrogen providing long-duration, resilience-oriented capacity—suggests that microgrid design standards and incentive structures should avoid treating storage as a monolithic category and instead differentiate support mechanisms by storage duration and application.

Second, the significant resilience gains achievable through coordinated EV charging and modest V2G participation (35% of fleet in this study) indicate that EV charging infrastructure should be designed from the outset with grid-interactive capability rather than as a purely unidirectional load, particularly in regions prone to extreme weather-related grid outages. Third, the sensitivity of optimal design to grid emission factor and discount rate assumptions underscores the importance of treating microgrid sizing as a dynamic rather than static exercise. As upstream grids decarbonize and financing conditions evolve, previously optimal configurations may no longer represent best-compromise solutions, motivating periodic re-optimization or the design of modular, expandable microgrid architectures that can be resized cost-effectively over time.

Finally, the steep marginal cost observed near very low LPSP and very high resilience index values suggests that policy targets mandating near-absolute reliability or resilience should be carefully weighed against their disproportionate cost implications, and that a multi-objective, stakeholder-informed selection process—such as the fuzzy decision-making approach applied here—offers a more defensible basis for design selection than arbitrary reliability targets.

## 10. Conclusion and Future Work

This paper has presented a multi-objective optimization framework for the integrated design of PV–fuel cell–hydrogen storage–EV charging microgrids, simultaneously addressing cost, emissions, reliability, and resilience objectives. An enhanced NSGA-II algorithm, incorporating chaotic initialization and adaptive genetic operators, was used to generate a well-distributed Pareto-optimal front, from which a best-compromise solution was selected via fuzzy decision-making. Applied to a representative community microgrid case study, the framework achieved an 18.6% reduction in total annualized cost, a 34.2% reduction in $CO_2$ emissions, an LPSP of 0.8%, and a 41.3% improvement in resilience index relative to conventional design baselines. Sensitivity analyses demonstrated the distinct roles of hydrogen storage (resilience-dominant), fuel cell power rating (peak-power-limited resilience), EV charging flexibility (cost-dominant), and external factors such as grid emission factor and discount rate in shaping optimal system configuration.

Future work should extend this framework in several directions: (1) incorporating stochastic and robust optimization techniques to explicitly account for uncertainty in solar irradiance, load growth, and hydrogen technology cost trajectories; (2) exploring multi-microgrid and networked resilience formulations where neighboring microgrids can share hydrogen and battery resources during contingency events; (3) integrating detailed degradation models for fuel cell stacks and batteries to more accurately capture long-term replacement costs under realistic cycling profiles; and (4) validating the framework against real-world pilot installations to assess the fidelity of the modeled resilience and reliability outcomes under actual outage events.

## References

[1]. Lopes, J. A. P., Moreira, C. L., & Madureira, A. G. (2006). Defining control strategies for microgrids islanded operation. *IEEE Transactions on Power Systems*.

[2]. Zhou, W., Lou, C., Li, Z., Lu, L., & Yang, H. (2010). Current status of research on optimum sizing of stand-alone hybrid solar–wind power generation systems. *Applied Energy*.

[3]. Nasser, M., Megahed, T. F., Ookawara, S., & Hassan, H. (2022). Techno-economic assessment of hydrogen storage systems for renewable energy applications. *International Journal of Hydrogen Energy*.

  

[4]. Deb, K., Pratap, A., Agarwal, S., & Meyarivan, T. (2002). A fast and elitist multiobjective genetic algorithm: NSGA-II. *IEEE Transactions on Evolutionary Computation*.

[5]. Fathy, A. (2019). Recent meta-heuristic grasshopper optimization algorithm for optimal reconfiguration of partially shaded PV array. *Solar Energy*.

[6]. Sadeghi, D., et al. (2021). Design and multi-objective optimization of a hybrid renewable microgrid with hydrogen storage. *Energy Conversion and Management.*

[7]. Xu, X., Hu, W., Cao, D., Huang, Q., Chen, C., & Chen, Z. (2020). Optimized sizing of a standalone PV-wind-hydrogen system considering economic dispatch. *Applied Energy*.

[8]. Mohandes, B., Moursi, M. S. E., Hatziargyriou, N., & Khatib, T. E. (2019). A review of power system flexibility with high penetration of renewables. *IEEE Transactions on Power Systems*.

[9]. Su, W., Wang, J., & Roh, J. (2014). Stochastic energy scheduling in microgrids with intermittent renewable energy resources. *IEEE Transactions on Smart Grid*.

[10]. Panwar, N. L., Kaushik, S. C., & Kothari, S. (2011). Role of renewable energy sources in environmental protection: A review. *Renewable and Sustainable Energy Reviews*.

[11]. Alavi, S. A., Ahmadian, A., & Aliakbar-Golkar, M. (2015). Optimal probabilistic energy management in a typical micro-grid based-on robust optimization and point estimate method. *Energy Conversion and Management*.

[12]. Amrollahi, M. H., & Bathaee, S. M. T. (2017). Techno-economic optimization of hybrid photovoltaic/wind generation together with battery storage system in a stand-alone micro-grid subjected to demand response. *Applied Energy*.

[13]. Li, B., Roche, R., Paire, D., & Miraoui, A. (2017). *Sizing of a stand-alone microgrid considering electric power, cooling/heating, hydrogen loads and hydrogen storage degradation*. Applied Energy, 205, 1244–1259.

[14]. Mah, A. X. Y., Ho, W. S., Hassim, M. H., Hashim, H., Ling, G. H. T., Ho, C. S., & Muis, Z. A. (2021). *Optimization of a standalone photovoltaic-based microgrid with electrical and hydrogen loads*. Energy, 235, 121386.

[15]. Diab, A. A. Z., Sultan, H. M., Mohamed, I. S., Kuznetsov, O., & Ton, D. D. (2019). *Application of Different Optimization Algorithms for Optimal Sizing of PV/Wind/Diesel/Battery Storage Stand-Alone Hybrid Microgrid*. IEEE Access, 7, 119223–119245.

[16]. Al-Shamma'a, A. A. (2022). *Optimal Sizing of a Hybrid Renewable Photovoltaic–Wind System-Based Microgrid Using Harris Hawk Optimizer*. International Journal of Photoenergy, 2022, Article 4825411.

[17]. Adoum Abdoulaye, M., Waita, S., Wekesa, C. W., & Mwabora, J. M. (2024). *Optimal sizing of an off-grid and grid-connected hybrid photovoltaic-wind system with battery and fuel cell storage system: A techno-economic, environmental, and social assessment*. Applied Energy, 365, 123201.

[18]. Reuß, M., Grube, T., Robinius, M., Preuster, P., Wasserscheid, P., & Stolten, D. (2017). *Seasonal storage and alternative carriers: A flexible hydrogen supply chain model*. Applied Energy, 200, 290–302.

[19]. Khiareddine, A., Ben Salah, C., Rekioua, D., & Mimouni, M. F. (2018). *Sizing methodology for hybrid photovoltaic/wind/hydrogen/battery integrated to energy management strategy for pumping system*. Energy, 153, 743–762.

[20]. Dawood, F., Shafiullah, G. M., & Anda, M. (2020). *Stand-Alone Microgrid with 100% Renewable Energy: A Case Study with Hybrid Solar PV–Battery–Hydrogen*. Sustainability, 12(5), 2047.

[21]. Li, B., Roche, R., & Miraoui, A. (2017). *Microgrid sizing with combined evolutionary algorithm and MILP unit commitment*. Applied Energy, 188, 547–562.

[22]. Wang, Y., Yi, Z., Shi, D., Yu, Z., Huang, B., & Wang, Z. (2018). *Optimal Distributed Energy Resources Sizing for Commercial Building Hybrid Microgrids*. arXiv:1803.00660.

[23]. Qi, N., Huang, K., Fan, Z., & Xu, B. (2024). *Long-Term Energy Management for Microgrid with Hybrid Hydrogen-Battery Energy Storage: A Prediction-Free Coordinated Optimization Framework*. arXiv:2407.21698.

[24]. Wang, J., Liu, C., Ton, D., Zhou, Y., Kim, J., & Vyas, A. (2011). *Impact of plug-in hybrid electric vehicles on power systems with demand response and wind power*. Energy Policy, 39(7), 4016–4021.

[25]. Erdinc, O., & Uzunoglu, M. (2012). *Optimum design of hybrid renewable energy systems: Overview of different approaches*. Renewable and Sustainable Energy Reviews, 16(3), 1412–1425.

[26]. Bahramirad, S., Reder, W., & Khodaei, A. (2012). *Reliability-constrained optimal sizing of energy storage system in a microgrid*. IEEE Transactions on Smart Grid, 3(4), 2056–2062.

[27]. Hatziargyriou, N. (Ed.). (2014). *Microgrids: Architectures and Control*. Wiley.

  